Available online at www.sciencedirect.com
ScienceDirect
Ceramics International 34 (2008) 1229–1236
CERAMICS INTERNATIONAL
www.elsevier.com/locate/ceramint

Fabrication of bulk nanocrystalline alumina–zirconia materials

Tomas Chraska *, Karel Neufuss, Jiří Dubský, Pavel Ctibor, Pavel Rohan

Institute of Plasma Physics, Academy of Sciences of the Czech Republic, Prague, Czech Republic

Received 3 November 2006; received in revised form 18 December 2006; accepted 1 March 2007
Available online 8 April 2007

Abstract

Eutectic mixtures of alumina and zirconia have been successfully transformed to thick amorphous coatings and free-standing parts by plasma spraying. The as-sprayed material has very low open porosity and crystallizes when heated above 950 °C. Short annealing times at the crystallization temperature result in the formation of a very fine microstructure throughout the sample volume with average grain size below 15 nm. The fine nanocomposite structure was confirmed by transmission electron microscopy. High hardness and abrasion resistance of the as-sprayed materials are significantly improved upon annealing due to the nanocomposite structure, which makes the bulk nanocrystalline ceramic material attractive.

Keywords: B: Nanocomposites; C: Wear resistance; D: Al_2O_3; D: ZrO_2

1. Introduction

Structural nanocrystalline ceramics are expected to posses significantly improved properties such as hardness, strength, abrasion resistance and to some extent toughness. However, limited ability to fabricate large three-dimensional parts (blocks, pipes, etc.) of compact nanocrystalline materials is the major obstacle for their greater use. There are many different techniques of fabricating nanocrystalline materials from solids, liquids, and vapors. Most of these techniques produce materials in the form of nanocrystalline powders (nanoparticles). Synthesis of large quantities of ceramic nanoparticles has been mastered but the consolidation of nanoparticles into mesoscopic structures and large bulk parts remains a challenge [1].

The powder consolidation process must allow retention of the nanometer grain size and at the same time bring residual porosity levels to a minimum. For the successful consolidation of ceramic nanomaterials to densities where the improvements in physical and mechanical properties can be exploited, processing techniques that rely on application of high pressure and raised consolidation temperatures are required. Raising the temperature causes undesirable grain growth and microstructure coarsening whereas low temperature is often not sufficient to achieve full inter-particle bonding and thus fully dense samples [2]. Moderate success has been achieved by so called Transformation Assisted Consolidation (TAC) [3], which takes advantage of a pressure-induced phase transformation to suppress grain growth during consolidation. TAC has been used to fabricate small compact samples of nano-TiO_2 and nano-Al_2O_3 with densities above 95% and with grain sizes as small as 25 nm and 49 nm, respectively [4,5].

An alternative method to produce bulk nanocrystalline materials is to avoid the powder compaction step altogether. One such way is to produce amorphous material (glassy phase) by rapid solidification and then by controlled crystallization introduce nanocrystalline structure [2]. Such material can be either fully nanocrystalline or in the form of a nanocomposite, in which the nanometric crystallites are dispersed in the original amorphous phase. One technique capable of achieving rapid solidification in materials is plasma spraying (PS). In the conventional PS process, powder particles (10–120 μm) are injected into a high temperature plasma jet generated by using plasma torch. Individual particles are quickly melted by the plasma and propelled onto a substrate where they spread upon impact and rapidly solidify due to high heat extraction by the cold substrate. The solidified discs are called splats and they represent the basic building blocks of a PS coating. Repetitive passing of the plasma torch over a substrate can produce

* Corresponding author at: Institute of Plasma Physics ASCR, Za Slovankou 3, 182 00 Prague 8, Czech Republic. Tel.: +420 266 053 307; fax: +420 286 586 389.
E-mail address: tchraska@ipp.cas.cz (T. Chraska).

0272-8842/$34.00
doi:10.1016/j.ceramint.2007.04.001

coatings from 0.1 mm to several millimeters thick. The extremely high cooling rates (10^3–10^6 K/s) in the impinged particles give rise to formation of nonequilibrium phases, microstructures of narrow columnar grains of nanometer dimensions [6], and amorphous phases (e.g. [7]).

Alumina–zirconia pseudobinary system contains a eutectic point at 58 wt.% (Fig. 1). It has been previously reported that material with near eutectic composition can solidify as amorphous or partially nanostructured solid due to rapid solidification [8,9]. The metastable amorphous material will crystallize during annealing [8].

This paper reports the successful fabrication of bulk nanocrystalline parts based on near eutectic alumina–zirconia materials by utilizing the water stabilized plasma torch (WSP®)[10]. The main advantages of the WSP® torch are high powder throughput (up to several tens of kilograms per hour) and very high plasma enthalpy, which makes the torch suitable even for high-volume production of thick coatings of high-melting-point ceramic materials. The WSP® can also be used for fabrication of a large variety of shapes of free-standing parts with wall thickness of 0.5 to over 10 mm. Plates, tubes, pipes (1.5 m long), bowls, crucibles have been fabricated by spraying different feedstock materials, such as alumina, mullite, zircon, garnet, basalt [11]. The WSP® torch is used in this work for the first time to prepare amorphous deposits and amorphous free-standing parts from alumina–zirconia near eutectic materials. Nanostructure develops as a result of crystallization during post-annealing of as-sprayed amorphous parts. Comparison of selected mechanical properties of as-sprayed and annealed samples is presented.

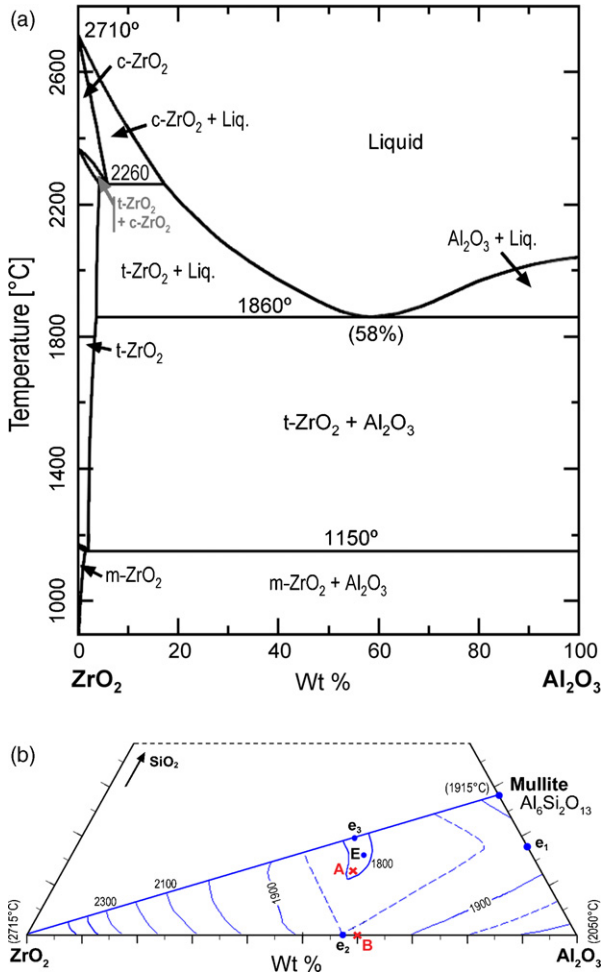

Fig. 1. (a) Binary equilibrium phase diagram of alumina–zirconia system [*ACerS-NIST Phase Equilibria Diagram, CD-ROM Database, Version 3.0*]. (b) Portion of ternary equilibrium phase diagram of alumina–zirconia–silica system [*ACerS-NIST Phase Equilibria Diagram*]. Approximate compositions of materials A and B denoted by crosses. Compositions of binary and ternary eutectics denoted by dots with letters e and E, respectively.

2. Experimental

Two slightly different feedstock powders were tested for plasma spraying using the WSP®. Powder A material contains about 15 wt.% of SiO_2 and up to 2.5 wt.% of alkaline-earth oxides (mostly Na_2O) in addition to the near eutectic ratio of Al_2O_3 and ZrO_2 compounds. This refractory material is available as cast tiles and linings and exhibits high hardness, high abrasion resistance, and extremely high chemical resistance. It is fabricated by melt casting followed by slow furnace cooling. Cast tiles of the material were crushed and sieved to obtain feedstock powder A with a sieved grain size of 40–63 μm. Powder B is a standard fused and crushed powder with nominal composition of 60 wt.% Al_2O_3 and 40 wt.% ZrO_2 and a sieved grain size range from 45 to 90 μm (Industriekeramik Hochrhein GmbH, material No. 1460). Both feedstock powders were plasma sprayed in air, at atmospheric pressure using the WSP 500® torch operating at 160 kW power. The powders were injected into the plasma jet by compressed air at a constant feed rate of about 250 g/min and deposited onto mild steel substrates positioned 350 mm away from the torch nozzle. Individual sprayed particles were monitored in flight by optical sensing device (DPV 2000) in order to determine their temperature, velocity, and size. The mild steel surfaces were either sand blasted to assist in the production of well-adhered thick coatings or treated for easy deposit removal from substrates to produce free-standing parts (e.g. 25 mm × 100 mm × 3 mm test coupons or pipes with 80 mm inner diameter and 2 mm thickness).

Selected free-standing samples were heat treated in air to 1200 °C at a heating rate of 5 K/min, held for 1 min and then cooled down to room temperature at a cooling rate of 5 K/min. The same heating cycle was applied in DTA equipment, dilatometer (TMA), and also in furnace to large free-standing samples. In order to better understand the crystallization and to produce nanocrystalline structure, additional heat treatments were carried out in air with heating and cooling rates fixed at 10 K/min and maximum temperature limited to the vicinity of the crystallization temperature.

Materialographic samples were prepared from free-standing parts, feedstock powders, and also from free-flight particles collected 1500 mm away from the nozzle. Microstructure was characterized by light microscopy and scanning electron microscopy (SEM) equipped with energy dispersive X-ray spectrometer (EDS). Thin foil cross-sectional samples for transmission electron microscope (TEM) were prepared by wedge polishing technique and short ion-mill exposures. The foil

samples were observed by conventional 200 kV TEM and 300 kV high-resolution TEM equipped with EDS. X-ray diffraction (XRD) was used to determine crystallinity and phase content of the bulk samples and line-profile analysis was employed to estimate crystallite size. Porosity was measured by Archimedean (water immersion) technique. Thermal properties were measured on finely crushed samples by differential thermal analysis (DTA) and on oblong parallelepiped samples by dilatometry (i.e. thermo mechanical analysis—TMA). Young's modulus of the as-sprayed coatings was calculated from the results of four point bend tests. Microhardness of the coatings was measured by optical microscope equipped with a Hanemann head [12] and Vickers indenter using 1 N load applied over 15 s. The mean value of microhardness was calculated as an average from 20 indentations. Finally, slurry abrasion response (SAR) tests were performed according to a modified ASTM G75 standard using alumina slurry.

3. Results and discussion

3.1. Feedstock powders

Both feedstock powders A and B are fully crystalline as determined by XRD. The following phases were identified in both powders: monoclinic ZrO_2 (baddeleyite), α-Al_2O_3 (corundum), and tetragonal ZrO_2 (t-ZrO_2). Powder A also exhibits a small peak that belongs to crystalline SiO_2 (quartz) (Fig. 2a).

SEM examination of materialographic samples of as-received powders revealed significant difference between the two powders. The individual particles of powder A always contain both of the main constituents (i.e. alumina and zirconia) embedded in a fine eutectic microstructure (Fig. 3), whereas the individual particles of powder B often comprise only one of the constituents. Image analysis revealed that only about 55% of powder B particles is made up of the fine eutectic microstructure, the rest being either pure alumina or zirconia particles, which points to a low quality manufacturing process of powder B.

It was confirmed by EDS that there are three chemically distinct regions within all powder A particles. Pure phases of Al_2O_3 and ZrO_2 are accompanied by regions of mixed Al and Si oxides with traces of Na, K, and Ca. The eutectic microstructure of powder A is often rather coarse due to the slow furnace cooling that follows casting of the original material.

3.2. Plasma spraying and individual splats

Both feedstock materials sprayed well with good deposition efficiency and very low open porosity. Average temperature of

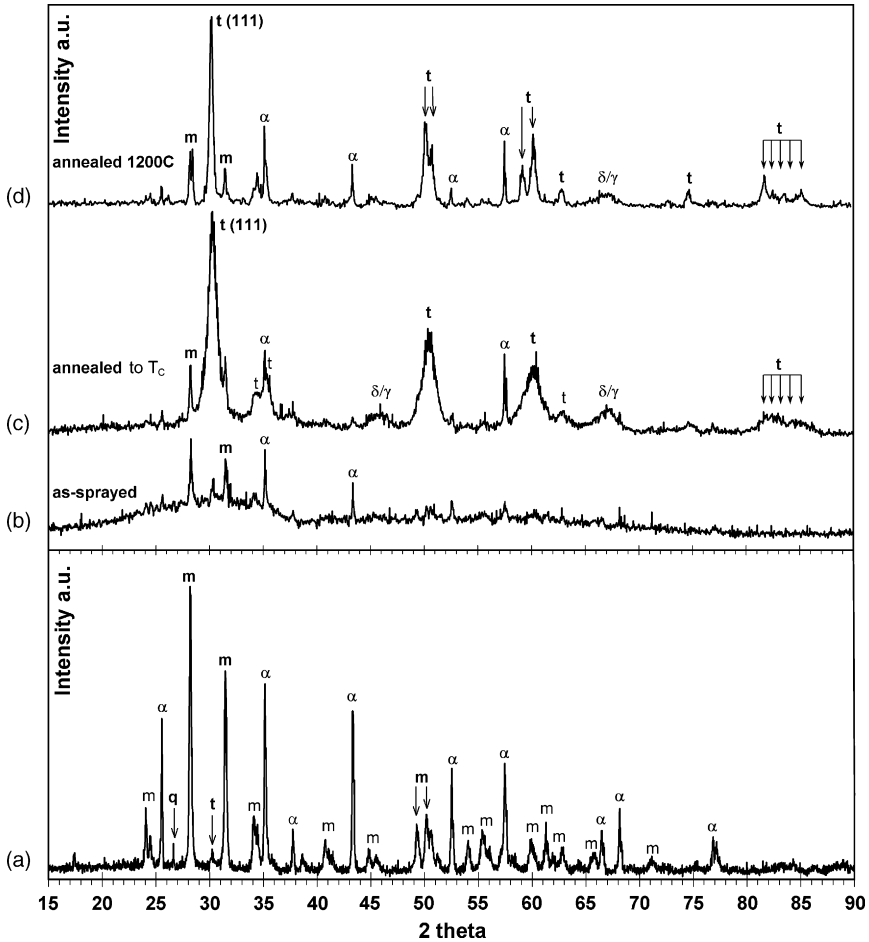

Fig. 2. XRD patterns of powder A feedstock (a), corresponding as-sprayed (b), annealed at T_C for 1 min (c), and annealed at 1200 °C for 1 min samples: m—monoclinic ZrO_2; t—tetragonal ZrO_2; δ/γ—delta and gamma metastable Al_2O_3; α—alpha Al_2O_3; q—quartz SiO_2 (d).

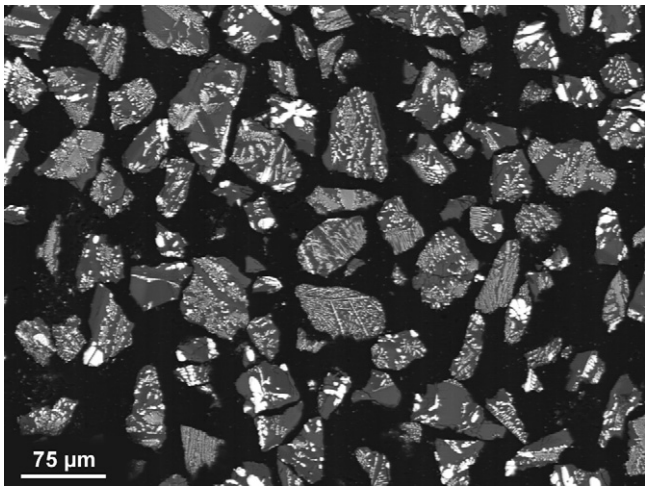

Fig. 3. SEM image (backscattered electrons) of un-etched polished cross-section of feedstock powder A embedded in epoxy (black regions). Zirconia is represented by white regions, alumina by gray regions.

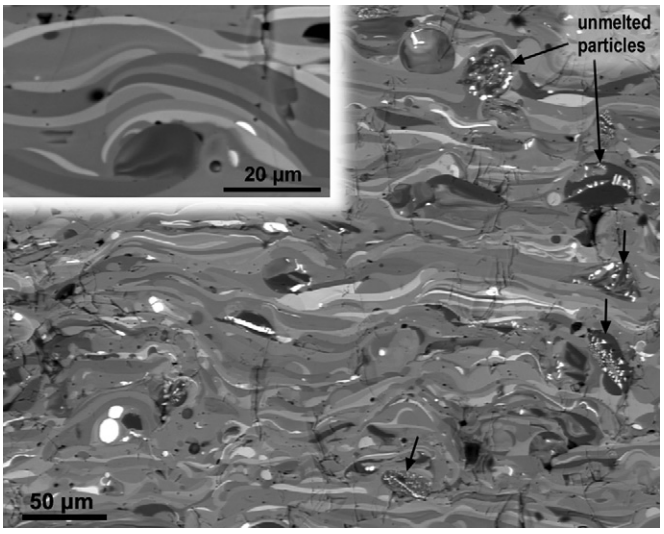

Fig. 4. SEM image (backscattered electrons): Materialographic cross-section of as-sprayed coating of feedstock A. Arrows point to unmelted particles. Inset picture shows a detail of the layered splat structure. See text for detailed description.

sprayed particles as recorded by DPV-2000 just before impacting the substrate was 2450 °C with a standard deviation of about 100 °C for all combinations of spraying parameters (measured only for powder A). The average velocity at impact was between 85 and 95 m/s with a standard deviation of about 17 m/s in all cases. Open porosity of the free-standing parts was found to be very low between 1.5 and 2% for powder A and between 3 and 3.5% for powder B.

Solidified free-flight particles of powder A were collected at a distance of 1500 mm from the torch nozzle. Most of the particles had been melted in the plasma. The molten particles are round and contain almost homogeneous blend of all the oxides present in the feedstock powder as determined by EDS. Some of the particles, however, are only partially melted and their internal microstructure is identical to the eutectic microstructure of the feedstock particles.

Material A was also sprayed at very low feeding rate on polished substrates preheated to 350 °C in order to prepare individual splats. The splats are circular with diameters ranging between 125 and 275 μm and thickness of 1.5–2.5 μm. The splats are contiguous with a smooth unbroken rim and no observable vertical cracks. That is unlike most splats of other ceramic materials that develop a net of vertical cracks during cooling after molten droplet impact and crystallization. The crack-less nature of material A splats is an advantage when it comes to mechanical properties of such coating. Cross-sectional TEM studies of the individual splats resolved them to be fully amorphous with no distinct microstructure. This is also unlike most splats of other ceramic materials that crystallize with narrow columnar grains which grow after copious nucleation due to large undercooling [6]. Each individual amorphous splat of material A is chemically homogeneous but there is significant chemical variation among individual splats. That means there is good mixing of the original oxide compounds in the molten state of individual particle during its flight and impact but there are different proportion of the compounds in each particle, as shown in the following section.

3.3. As-sprayed samples—feedstock A

XRD analysis established the as-sprayed samples of feedstock A to be mostly amorphous (Fig. 2b). Crystallites of monoclinic and t-ZrO_2 and α-Al_2O_3 were also present in the as-sprayed samples. The samples appeared to be brittle during materialographic preparations. Typical microstructure of as-sprayed samples with just a few visible cracks is presented in Fig. 4. Image analysis determined that about 93% of the sample consists of thin splats and the remaining 7% are round particles. The splats contain a homogeneous blend of Alumina, Zirconia and Si oxide. Different proportions of Al and Zr oxides in the individual feedstock particles, result in different concentrations of Al and Zr oxides in the blended splats, which in turn corresponds to various shades of gray in Fig. 4. Chemical distribution of elements in the round particles with the segregated microstructure matches exactly that of the feedstock powder (Section 3.1). Therefore, these regions are the unmelted remains of the feedstock particles with eutectic microstructure and represent about 7% of the sample. The blended splats are amorphous as was confirmed by TEM (Fig. 5) whereas the unmelted particles are crystalline, giving rise to the small XRD peaks (Fig. 2b). Therefore, about 93% of the as-sprayed coatings are made of amorphous splats. Each of the amorphous splats is a homogeneous supersaturated solid solution of the main oxides, which did not crystallize to form eutectic microstructure due to rapid solidification during plasma spraying.

3.4. As-sprayed samples—feedstock B

Due to the high fraction of particles containing only pure monoclinic ZrO_2 or α-Al_2O_3, the as-sprayed samples of feedstock B contain correspondingly lower fraction of amorphous material. The pure alumina or zirconia splats

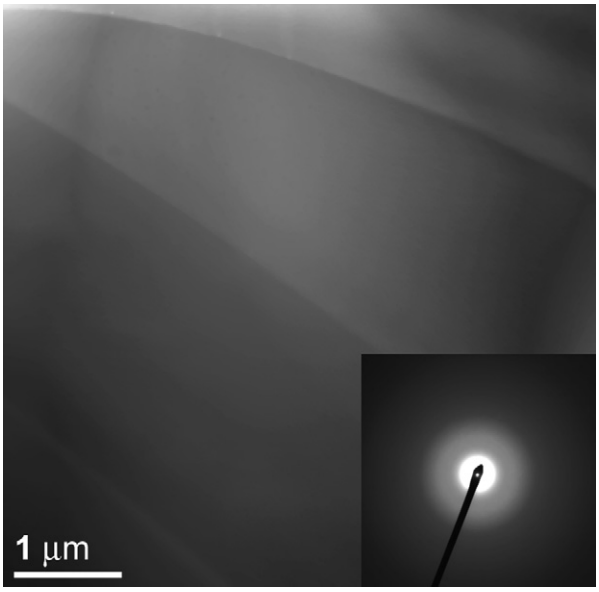

Fig. 5. Bright field TEM image of four amorphous splats in as-sprayed coating. Corresponding selected area diffraction pattern is in the inset.

undergo crystallization during splat solidification, which leads to standard columnar grain microstructure [6]. There is therefore smaller number of amorphous splats in the coating. This is clearly manifested on the XRD pattern (Fig. 6). Most of the pure α-Al_2O_3 feedstock particles transformed upon spraying to metastable γ/δ-Al_2O_3 splats, which is a typical result for plasma sprayed alumina [13]. Significant fraction of the monoclinic ZrO_2 particles transformed to t-ZrO_2. Analysis of SEM images established that less than 50% of the sample consists of splats containing a homogeneous blend of Al and Zr oxides, almost 10% are unmelted particles and the rest are pure alumina or zirconia splats, which are crystalline. Only the blended splats are amorphous, which is analogous to the as-sprayed result of feedstock A.

3.5. Heat treatment—feedstock A

The DTA measurement during two consecutive identical heating runs indicates crystallization during the first run with the onset of exothermic transformation just above 950 °C (further referred to as crystallization temperature T_C). During the DTA measurement, thermo-gravimetrical data was also collected. There was no change of sample weight during the run indicating that the phases in the as-sprayed material are stoichiometric with respect to their oxygen content. TMA measurement confirmed the onset of crystallization above 950 °C and produced a material shrinkage of 1.7% during crystallization. This shrinkage was attributed to the higher number of cracks observed by light microscopy and SEM in the annealed samples. EDS analyses of annealed samples confirmed that the local chemical distribution is identical to that of the as-sprayed material. No microstructural difference was detected in the annealed samples probably due to limited resolution of the SEM equipment. No amorphous phases were detected by XRD in the samples annealed to 1200 °C (Fig. 2d). The heat-treated material is fully crystalline and contains primarily tetragonal zirconia. Peaks of monoclinic ZrO_2 and α-Al_2O_3 were also identified.

In order to better understand the crystallization and to produce nanocrystalline structure, additional heat treatments were carried out in air with heating and cooling rates fixed at 10 K/min and short dwell times at the vicinity of the crystallization temperature T_C, i.e. about 950 °C. One set of as-sprayed samples was heated to T_C and cooled after only a short dwell time. XRD pattern of the annealed sample is presented in Fig. 2c. Peak heights of the monoclinic ZrO_2 phase in the annealed sample corresponds to those of the as-sprayed coating (Fig. 2b). Therefore, the monoclinic phase is located almost exclusively in the partially melted particles. Conversely, the predominant t-ZrO_2 and gamma/delta Al_2O_3 phases crystallize simultaneously within the amorphous splats. Each splat is a homogeneous blend of the main oxides, but there are appreciable chemical variations going from one splat to another (as shown in Section 3.3).

Crystallite size was estimated using only the (1 1 1) tetragonal line by means of the shape factor method. Remaining tetragonal lines overlap with several lines of the other identified phases thus rendering them unsuitable for line fitting and analysis. Instrumental broadening of the X-ray machine was subtracted and Cu $K_{\alpha 1}$ peak deconvolution was carried out.

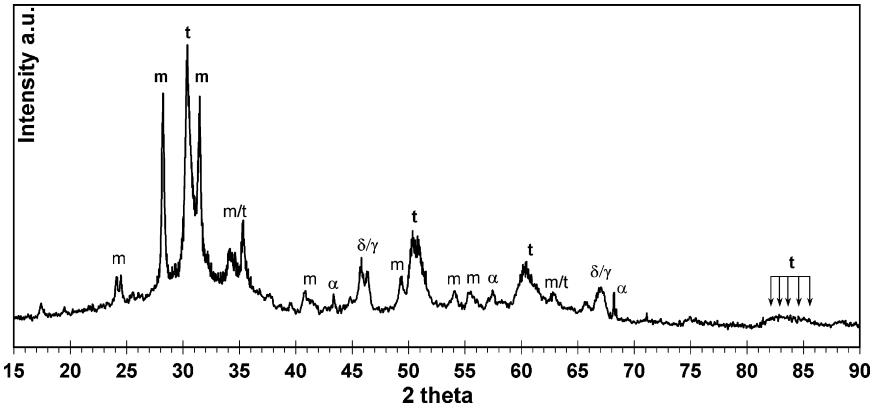

Fig. 6. XRD pattern of as-sprayed sample of feedstock powder B: m—monoclinic ZrO_2; t—tetragonal ZrO_2; δ/γ—delta and gamma metastable Al_2O_3; α—alpha Al_2O_3.

Table 1
Crystallite size in annealed samples

Annealing T (°C)	Crystallite size (nm)	
	TEM	XRD
960	12.5	13
1200	34	40

Results of the XRD line width analysis with corresponding crystallite sizes of the t-ZrO_2 are presented in Table 1. The small γ and δ alumina lines (Fig. 2) are also very wide. It is obvious from these results, that the heat-treated samples are nanocrystalline within their entire volume with the exception of the 7% of unmelted particles (Section 3.3). The unmelted particles were not affected by heat treatment and remained crystalline and coarse-grained. Verification of the fine microstructure was carried out in TEM (Fig. 7a) and high-resolution TEM (Fig. 7b). Several hundreds of nanocrystalline grains were analyzed on several TEM micrographs. The TEM results are in good agreement with the XRD line width analysis (Table 1). Raising the annealing temperature above the crystallization temperature T_C brings about slow grain coarsening of the extremely fine microstructure.

Detailed observations of bright field TEM images reveals a fine network of a weak contrast phase in between the individual t-ZrO_2 grains (Fig. 7a). The grains appear to be rounded rather than jagged or angular and do not form grain boundaries. The predominant t-ZrO_2 grains are embedded in remains of the amorphous matrix, which may have partially transformed to γ/δ-Al_2O_3 phase. Therefore, the heat treatment at the transformation temperature produces a structure best described as nanocomposite with average crystallite size of 13 nm and inter-crystallite network. It is also interesting to note the microstructural differences between individual splats (Fig. 8) arising due to the different percentages of alumina and silica present in each splat. TEM image analysis combined with EDS analysis reveals that higher fraction of silica within a splat tends to produce larger nanocrystallites and thicker inter-crystallite network.

It is interesting to note that although alumina comprises more than half of the volume of the feedstock material the α-Al_2O_3 peaks of the annealed material are very small even when we consider poor scattering of this phase. The XRD pattern also contains small peaks of gamma and/or delta Al_2O_3, which could be partly due to transformation of α-Al_2O_3 and partly due to crystallization within the amorphous splats. The newly formed gamma and/or delta Al_2O_3 peaks are also much smaller than the dominant t-ZrO_2 peaks. The predominance of t-ZrO_2 could be explained by significantly extended solid solubility of alumina in tetragonal zirconia compared to that predicted by equilibrium phase diagram (Fig. 1). Ternary phase diagram (Fig. 1b) predicts mullite as the third equilibrium phase but this phase was not detected and thus SiO_2 can be both dissolved in the inter-crystallite phase and in the t-ZrO_2 solid solution crystallites. The presumption of extended solid solubility is further corroborated by the observed systematic shift of tetragonal peaks toward higher angles. Radii of the Al and Si atoms are smaller than that of Zr atom and thus the tetragonal lattice shrinks when Zr atoms are substituted by Al and Si atoms and hence the d-spacings decrease. Supersaturated t-ZrO_2 with Al_2O_3 has been already reported by several investigators in the case of binary alumina–zirconia materials (e.g. [9,14]). The nanocomposite material reported in this work is far from equilibrium. Comparing the XRD patterns of samples annealed to T_C and 1200 °C (Fig. 2) reveals that further heating causes first of all the decrease of gamma and delta alumina which transform to alpha alumina and secondly the decrease of tetragonal peak widths, which corresponds to grain coarsening and internal stress relaxation. In addition, no inter-crystalline network was observed on TEM images of samples annealed to 1200 °C.

As-sprayed samples of feedstock B were also heat treated above 1000 °C. TMA measurement confirmed the onset of

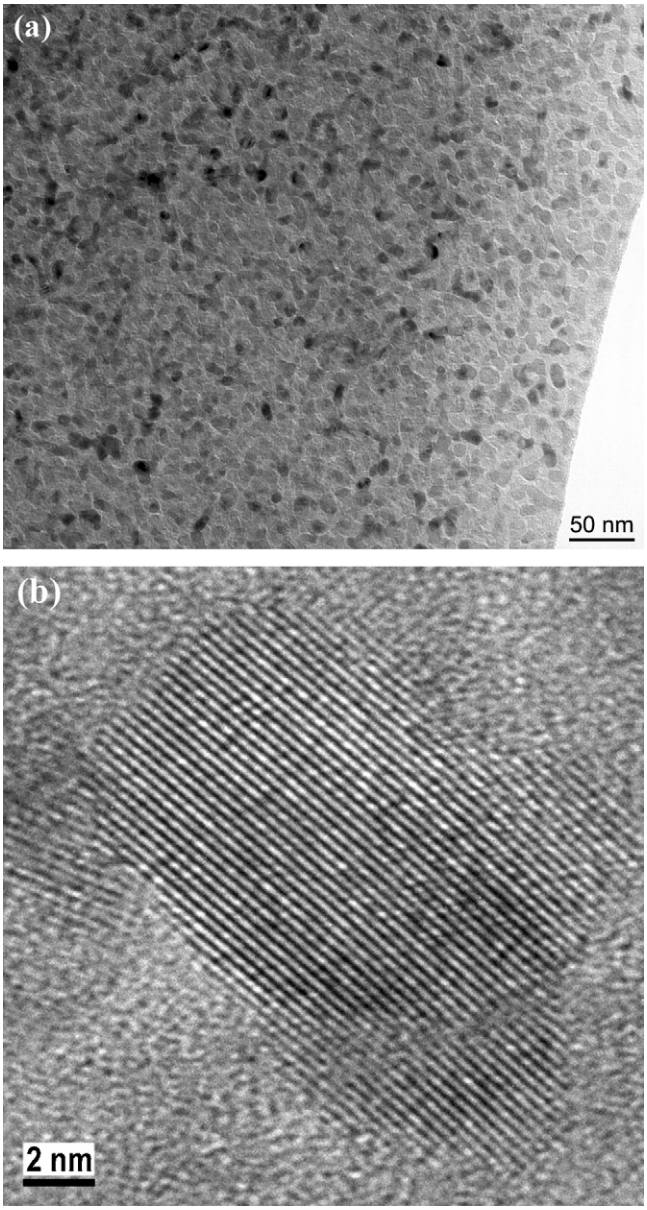

Fig. 7. (a) Bright field TEM image of nanocrystalline grains in annealed sample. (b) HRTEM image of nanocrystalline grain of tetragonal zirconia.

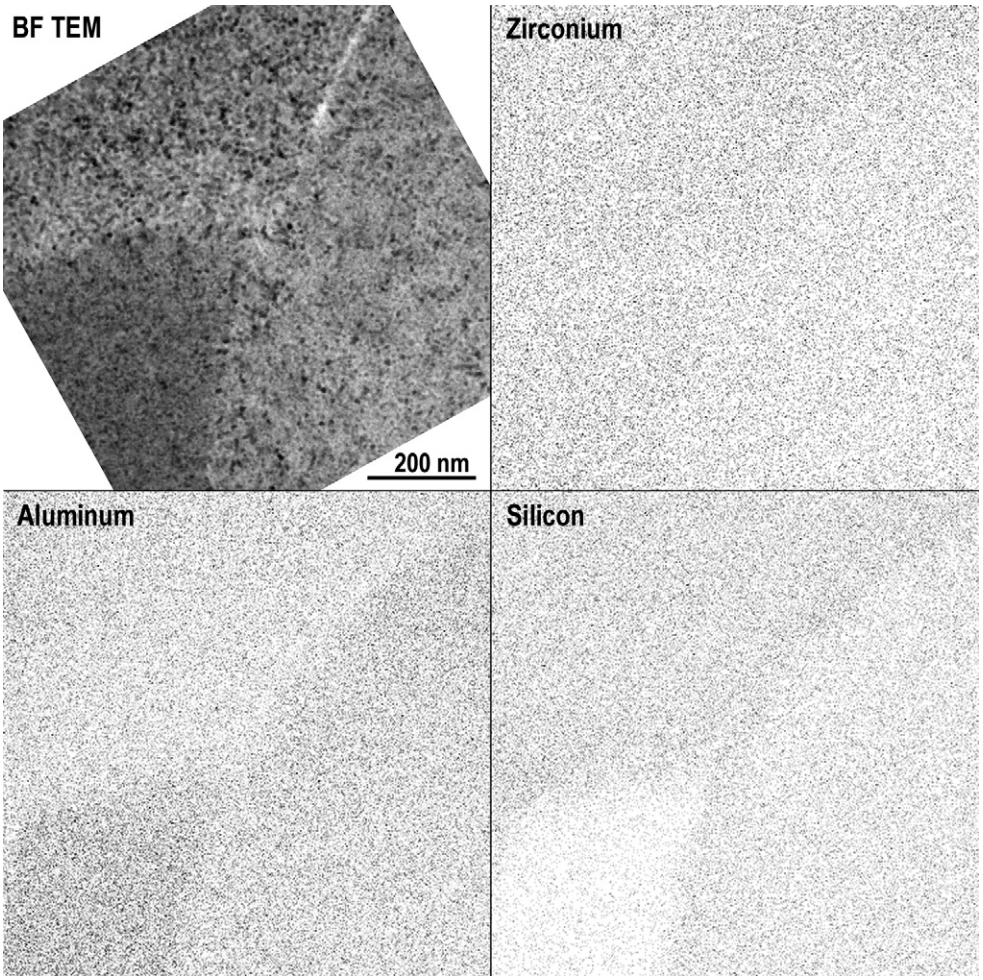

Fig. 8. Bright field TEM image of three adjacent splats and corresponding Zr, Al, and Si elemental maps by EDS.

crystallization above 950 °C (the same as for material A) and a measured material shrinkage of only 0.35% during the crystallization. The low crystallization shrinkage is related to the low amorphous content of the as-sprayed material. Therefore, samples of material B were excluded from further treatments and studies due to their low amorphous and nanocrystalline content.

3.6. Mechanical properties—material A

Well-adhered coatings on carbon steel substrates (25 mm × 120 mm) were subject to four point bend to determine Young's modulus. Coatings of 1.4 mm thickness on 3 mm thick substrate were first bent four times in compression and then four times in tension. The bend test data were used to calculate average value of Young's modulus of the as-sprayed coating in compression and tension. The test yielded values of 35 GPa in compression and 26 GPa in tension. These values are comparable to those of pure alumina coatings [15] and slightly higher than those of thermal barrier coatings prepared by air plasma spraying [16]. In general, Young's modulus in tension tends to be lower than that in compression for plasma sprayed coatings due to the ease with which the microcracks in the coating are opened.

Microhardness measurements of as-sprayed and annealed coatings, as measured by Vickers indenter, are summarized in Table 2. The lowest microhardness was measured for the as-sprayed sample. Significant increase of hardness values in samples annealed for 1 min at the transformation temperature T_C can be attributed to the fine nanocrystalline microstructure. Such an increase is principally in accordance with the Hall–Petch relationship.

Slurry abrasion response (SAR) tests were performed for as-sprayed and annealed (T_C) samples of material A according to a modified ASTM G75 standard. In each case, four samples (12 mm × 25 mm) were slid back and forth on rubber strips immersed in slurry of fine alumina powder and water. Weight loss had been measured four times after 2 h intervals which correspond to ∼2000 m sliding distance. Average volume loss

Table 2
Results of microhardness and SAR tests of various samples

Sample	HV (GPa)	Wear rate (mm^3/km)
As-cast material	n/a	4.6 ± 1.3
As-sprayed	12.84 ± 0.94	6.1 ± 0.6
Annealed to T_C	16.52 ± 1.81	2.9 ±0.5
Annealed to 1200 °C	13.74 ± 1.33	n/a

after each interval was calculated using sample density. The slope of linear interpolation of the four measured points determines the overall abrasion loss and for the as-sprayed coating it is equal to 6.1 mm^3 per 1000 meters of sliding (Table 2). This value is comparable to that of pure alumina coatings. Samples annealed to the crystallization temperature exhibit significant improvement of the abrasion resistance. The value of 2.9 mm^3 per 1000 m is exceeded only by that of chromium oxide sprayed by WSP® (2.5 mm^3 per 1000 m [17]). The improvement of abrasion resistance is consistent with the hardness increase and can both be attributed to the fine nanocrystalline structure of the heat-treated samples.

3.7. Summary and conclusion

Deposits and free-standing parts of two ceramic materials have been plasma sprayed by WSP® with very low open porosity. Material A contained about 15 wt.% of SiO_2 and up to 2.5 wt.% of alkaline-earth oxides in addition to the near eutectic ratio of Al_2O_3 and ZrO_2 compounds. All powder particles of material A contain both alumina and zirconia compounds. Feedstock material B had nominal eutectic composition of 60 wt.% Al_2O_3 and 40 wt.% ZrO_2, yet was strongly inhomogeneous containing significant amount of pure alumina and pure zirconia particles.

Plasma spraying of powder A resulted in 93% amorphous deposit. The as-sprayed deposits of material B contained less than 50% of amorphous splats and over 40% of crystalline splats of pure alumina or zirconia. The remaining 7% and 10% are accounted to unmelted particles in the as-sprayed deposits of material A and B, respectively. The amorphous content of the as-sprayed deposits is due to rapid solidification of powder particles possessing both alumina and zirconia compounds. Each of the amorphous splats is a homogeneous supersaturated solid solution of the main oxides, but there is significant chemical variation among individual splats.

Amorphous content of the as-sprayed deposits crystallizes just above 950 °C with an associated volume shrinkage of 1.8% and 0.35% for material A and B, respectively. The volume shrinkage does not cause material breakup.

Short heat treatment of the as-sprayed material A to the crystallization temperature produces a very fine nanocomposite structure within each splat. The crystallites with average size of 13 nm are embedded in fine inter-crystallite network. Each nanocrystallite is an extended solid solution of alumina and silica in tetragonal zirconia crystal structure. Precise details concerning the spraying parameters and the heat treatment procedure of material A are subject to a patent application [18].

Microhardness and abrasion resistance values determined for the as-sprayed material A are among the best of the ceramic materials sprayed using WSP®. Significantly higher values of both properties were measured on the annealed nanocrystalline samples. Abrasion resistance of the samples annealed to T_C is extremely high and comparable to that of pure chromia sprayed by WSP® [17].

In conclusion, feedstock powder A is a promising, high abrasion-resistant material that can be efficiently plasma sprayed to form amorphous coatings or free-standing parts. Heat treatment of the amorphous free-standing parts to the crystallization temperature leads to development of bulk nanocrystalline parts with additional improvement of the abrasion resistance.

Acknowledgements

Supported in part by ANCEC a joint project of the Academy of Sciences of the Czech Republic and National Research Council Canada. Electron microscopy studies were supported by the Czech Science Foundation, under Grant No. 106/04/P012.

References

[1] M. Winterer, Nanocrystalline Ceramics: Synthesis and Structure. Springer Series in Materials Science, vol. 53, Springer, Berlin - New York, 2002.
[2] C. Suryanarayana, The structure and properties of nanocrystalline materials: issues and concerns, JOM-J. Miner. Met. Mater. Soc. 54 (9) (2002) 24–27.
[3] B.H. Kear, J. Colaizzi, W.E. Mayo, S.C. Liao, On the processing of nanocrystalline and nanocomposite ceramics, Scripta Mater. 44 (8–9) (2001) 2065–2068.
[4] S.C. Liao, Y.J. Chen, W.E. Mayo, B.H. Kear, Transformation-assisted consolidation of bulk nanocrystalline TiO_2, Nanostruct. Mater. 11 (4) (1999) 553–557.
[5] S.C. Liao, Y.J. Chen, B.H. Kear, W.E. Mayo, High pressure low temperature sintering of nanocrystalline alumina, Nanostruct. Mater. 10 (6) (1998) 1063–1079.
[6] T. Chraska, A.H. King, Transmission electron microscopy study of rapid solidification of plasma sprayed zirconia—part II. Interfaces and subsequent splat solidification, Thin Solid Films 397 (1/2) (2001) 40–48.
[7] K. Neufuss, J. Ilavsky, J. Dubsky, B.J. Kolman, P. Chráska, Plasma spraying of silicates II, in: Proceedings of the United Thermal Spray Conference, 1999, pp. 636–640.
[8] H.J. Kim, Y.J. Kim, Amorphous phase formation of the pseudo-binary Al_2O_3–ZrO_2 alloy during plasma spray processing, J. Mater. Sci. 34 (1) (1999) 29–33.
[9] X.Z. Zhou, V. Shukla, W.R. Cannon, B.H. Kear, Metastable phase formation in plasma-sprayed ZrO_2 (Y_2O_3)–Al_2O_3, J. Am. Ceram. Soc. 86 (8) (2003) 1415–1420.
[10] ELMES, s.r.o., Praha, Czech Republic, http://www.elmes.net/
[11] K. Neufuss, P. Chráska, B. Kolman, S. Sampath, Z. Trávniček, Properties of plasma-sprayed freestanding ceramic parts, J. Therm. Spray Technol. 6 (4) (1997) 434–438.
[12] H. Hanemann, E.O. Bernhardt, Ein Mikrohärteprüfer, Z. Metallkd. 32 (2) (1940) 35–38.
[13] R. McPherson, On the formation of thermally sprayed alumina coatings, J. Mater. Sci. 15 (1980) 3141–3149.
[14] T. Ando, Y. Shiohara, Metastable alumina structures in melt-extracted alumina-25 wt-percent zirconia and alumina-42 wt-percent zirconia ceramics, J. Am. Ceram. Soc. 74 (2) (1991) 410–417.
[15] O. Kovarik, J. Siegl, J. Nohava, P. Chraska, Young's Modulus, Fatigue behavior of plasma-sprayed alumina coatings, J. Therm. Spray Technol. 14 (2) (2005) 231–238.
[16] S. Patsias, N. Tassini, K. Lambrinou, Ceramic coatings: effect of deposition method on damping and modulus of elasticity for yttria-stabilized zirconia, Mater. Sci. Eng. A 442 (2006) 504–508.
[17] J. Nohava, P. Chráska, in: Proceedings of the International Symposium on Plasma Chemistry, 2003. CD-ROM.
[18] Patent application filed with the Czech Patent and Trademark Office.